

SCIENTIFIC REPORTS



OPEN

Generation of heterozygous fibrillin-1 mutant cloned pigs from genome-edited foetal fibroblasts

Received: 29 October 2015

Accepted: 29 March 2016

Published: 14 April 2016

Kazuhiro Umeyama^{1,2}, Kota Watanabe³, Masahito Watanabe^{1,2}, Keisuke Horiuchi^{3,4}, Kazuaki Nakano², Masateru Kitashiro³, Hitomi Matsunari^{1,2}, Tokuhiko Kimura^{5,†}, Yoshimi Arima⁶, Oltea Sampetean⁶, Masaki Nagaya¹, Masahiro Saito⁷, Hideyuki Saya⁶, Kenjiro Kosaki⁸, Hiroshi Nagashima^{1,2} & Morio Matsumoto³

Marfan syndrome (MFS) is an autosomal dominant genetic disease caused by abnormal formation of the extracellular matrix with an incidence of 1 in 3,000 to 5,000. Patients with Marfan syndrome experience poor quality of life caused by skeletal disorders such as scoliosis, and they are at high risk of sudden death from cardiovascular impairment. Suitable animal models of MFS are essential for conquering this intractable disease. In particular, studies employing pig models will likely provide valuable information that can be extrapolated to humans because of the physiological and anatomical similarities between the two species. Here we describe the generation of heterozygous fibrillin-1 (*FBN1*) mutant cloned pigs (+/Glu433AsnfsX98) using genome editing and somatic cell nuclear transfer technologies. The *FBN1* mutant pigs exhibited phenotypes resembling those of humans with MFS, such as scoliosis, pectus excavatum, delayed mineralization of the epiphysis and disrupted structure of elastic fibres of the aortic medial tissue. These findings indicate the value of *FBN1* mutant pigs as a model for understanding the pathogenesis of MFS and for developing treatments.

FBN1 encodes fibrillin-1 (FBN1), which is a 350-kDa glycoprotein comprising 2,871 amino acid residues. FBN1 is the principal structural component of extracellular microfibrils^{1–3} and is distributed throughout the body as a connective-tissue matrix of tissues such as skin, lung, kidney, vessels, cartilage, tendon, muscle, cornea, and ciliary zonule¹. FBN1 is intimately involved in the transforming growth factor- β (TGF- β) signalling pathway, which is essential for cell proliferation and differentiation. TGF- β 1 binds to fibrillin-1 via the latent TGF- β -binding protein (LTBP) and controls signalling through this pathway by inhibiting the binding of TGF- β 1 to its receptor^{4,5}.

Marfan syndrome (MFS) (OMIM #154700) is an autosomal-dominant disorder of connective tissue caused by mutations of *FBN1*^{6,7}. The symptoms of MFS manifest principally as cardiovascular and skeletal abnormalities. The primary cause of death of patients with MFS is progressive aortic dilation, principally in the sinus of Valsalva, leading to aortic dissection or rupture^{8,9}. Skeletal symptoms include a tall and thin physique, long limbs, arachnodactyly, thoracic deformity (pectus carinatum, pectus excavatum), scoliosis, a high-arched palate, and chronic joint laxity. Other symptoms include ectopia lentis and myopia, skin striae atrophicae, and recurrent hernia or pneumothorax^{8,9}.

Studies of *FBN1* mutant mice^{10–14} have contributed valuable information regarding the causes of MFS and for the development of treatments. However, small animals such as rodents are inadequate as models for humans to guide development of treatments involving surgical techniques to address cardiovascular or skeletal system

¹Meiji University International Institute for Bio-Resource Research, Kawasaki, 214–8571, Japan. ²Laboratory of Developmental Engineering, Department of Life Sciences, School of Agriculture, Meiji University, Kawasaki, 214–8571, Japan. ³Department of Orthopaedic Surgery, Keio University School of Medicine, Tokyo, 160–8582, Japan. ⁴Anti-aging Orthopaedic Research, Keio University School of Medicine, Tokyo, 160–8582, Japan. ⁵Department of Pathology, Keio University School of Medicine, Tokyo, 160–8582, Japan. ⁶Division of Gene Regulation, Institute for Advanced Medical Research, Keio University School of Medicine, Tokyo, 160–8582, Japan. ⁷Division of Operative Dentistry, Department of Restorative Dentistry, Tohoku University Graduate School of Dentistry, Sendai, 980–8575, Japan. ⁸Center for Medical Genetics, Keio University School of Medicine, Tokyo, 160–8582, Japan. [†]Present address: Department of Pathology, Yamaguchi University Graduate School of Medicine, Ube-shi, 755-8505, Japan. Correspondence and requests for materials should be addressed to H.N. (email: hnagas@meiji.ac.jp) or M.M. (email: morio@a5.keio.jp)

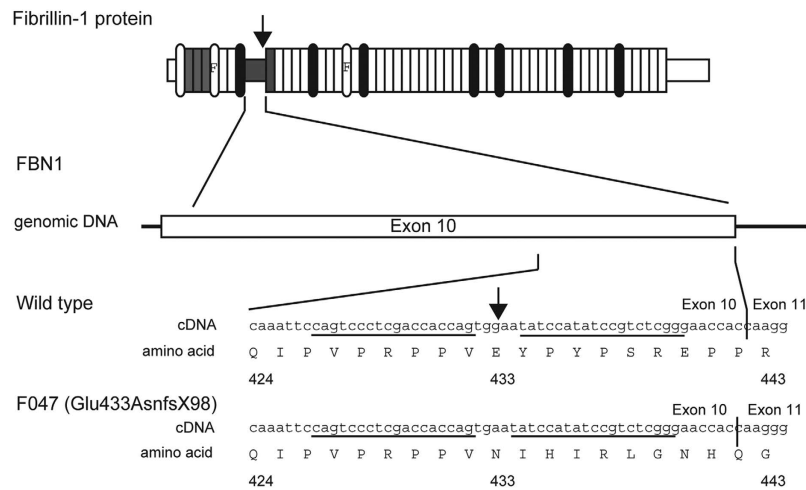


Figure 1. Schematic representation of porcine *FBN1* showing the cleavage site for the zinc finger nuclease *FBN1ZFN05*. Arrows indicate the cleavage sites for the ZFN. The ZFN recognition sequence is underlined.

manifestations. Therefore, large animals exhibiting a phenotype similar to the cardiovascular and skeletal manifestations of patients with MFS may contribute to the development of new treatments of patients with MFS and for gaining further insights into the pathogenesis of this intractable disease.

The application of recently developed genome editing and somatic cell cloning techniques has markedly improved the efficiency of generating pigs with gene mutations^{15–24}. In the present study, we generated heterozygous *FBN1* mutant cloned pigs and their progeny, and showed that they developed phenotypes resembling those of patients with MFS.

Results

Generation of heterozygous *FBN1* mutant cell lines. We used electroporation to introduce an mRNA encoding the zinc finger nuclease (ZFN) *FBN1ZFN05* that targets exon 10 of *FBN1*, which encodes a proline-rich region C (Fig. 1). Seven and 13 clones of homozygous and heterozygous mutants, respectively, which were isolated from 480 colonies, did not display detectable changes in cell shape or proliferation compared with the parental cells (Table 1). We selected the heterozygous *FBN1* mutant clone F047 (+/Glu433AsnfsX98), which encodes a putative truncated *FBN1* caused by a 1-bp deletion of a guanine nucleotide that creates a stop codon at amino acid residue 531 (Fig. 1, Fig. S1), to serve as the nuclear donor.

Generation of cloned piglets with a heterozygous mutant of *FBN1*. *FBN1* mutant cloned piglets with syngeneic backgrounds were created from embryos reconstructed via somatic cell nuclear transfer (SCNT) of heterozygous *FBN1* mutant cells (F047).

In the first experiment, we confirmed that 62.0% (245/395) of the SCNT embryos could develop to the blastocyst stage after *in vitro* culture for 5–6 days. The cloned blastocysts obtained were transferred into two recipients (103 embryos/recipient), and both recipients carried their pregnancies through birth, bearing seven live and one dead offspring (Table 2).

In the second experiment, 334 of the SCNT embryos were cultured *in vitro* for 1–2 days, and 272 embryos at the 1- to 2-cell stage were then transferred into two recipient gilts (136 embryos/recipient). Both recipients became pregnant, and they farrowed a total of 10 live and one stillborn piglets (Table 2).

In both experiments, the efficiencies of generating *FBN1* mutant cloned piglets from SCNT embryos (8/206, 3.9% and 11/272, 4.0%) were within the range of those normally achieved by our laboratory (1.4–4.3%)^{25–27}. All *FBN1* mutant cloned piglets harboured the same *FBN1* mutation and were the same sex as the F047 nuclear donor cells (Fig. S1). However, the phenotypes of the *FBN1* mutant cloned pigs obtained in the two experiments differed strikingly as described below.

Phenotypes of heterozygous *FBN1* mutant cloned pigs derived from blastocysts. Phenotypic abnormalities in the *FBN1* mutant cloned pigs obtained after transfer of the cloned blastocysts are presented in Table 3. Of the 8 neonatal piglets (including 1 stillborn), 3 exhibited external abnormalities including pectus excavatum (Fig. 2E) or cleft palate (Fig. S2). One of these animals showed both abnormalities.

Four piglets were analysed for skeletal abnormalities by computed tomography (CT) within 3 days after birth. Delayed mineralization in the epiphysis of the os coxa, femur, tibia, fibula, and humerus (Fig. 2G,H) was observed in one animal. Furthermore, the thoraxes of the mutant piglets were nearly conical, whereas the thoraxes of the WT piglets were barrel-shaped. No abnormalities of the spine were observed (Fig. 2B,F).

Aortic abnormalities were also detected in some of the *FBN1* mutant animals following Elastica van Gieson (EVG) staining of the wall tissue of the proximal thoracic aorta (Fig. 3). The aortic media of the control WT pigs contained a large number of wavy elastic fibres arranged vertically in an orderly structure (Fig. 3A,B). Extensive collagenous connective tissue that stained red was detected between these elastic fibres (Fig. 3A,B). In contrast,

Wild type genomic DNA		
	CAGTCCCTCGACCACCAGTGAATATCCATATCCGTCTCGG	
FBN1ZFN05 binding sequence		
	CAGTCCCTCGACCACCAGnnnnnTATCCATATCCGTCTCGG	
Homozygous mutants		
F038	CAGTCCCTCGACCACCAG****TATCCATATCCGTCTCGG	5bp del
F063	CAGTCCCTCGACCA*****TCCATATCCGTCTCGG	11bp del
F162	CAGTCCCTCGACCA*****TATCCGTCTCGG	15bp del
F007	CAGTCCCTCGACCACCAG <u>ACGG</u> ATATCCATATCCGTCTCGG	4bp sub
	CAGTCCCTCGACCAC*****ATATCCGTCTCGG	13bp del
F022	CAGTCCCTCGACCACCAG****ATATCCATATCCGTCTCGG	4bp del
	CAGTCCCTCGACC****TGAATATCCATATCCGTCTCGG	5bp del
F083	CAGTCCCTCGACCAC****GGAATATCCATATCCGTCTCGG	4bp del
	CAGTCCCTCGACC*****CATATCCGTCTCGG	14bp del
F117	CAGTCCCTCGACCACCA*****TATCCGTCTCGG	12bp del
	CAGTCCCTCGACCACCAG*****TCCGTCTCGG	13bp del
Heterozygous mutants		
F002	CAGTCCCTCGACCACCA*** <u>(111bp del)</u> **TAAAGTCA	111bp del
F005	CAGTCCCTCGACCACCAGTGGAT <u>GGAA</u> ATATCCATATCCGTCTCGG	4bp ins
F013	CAGTCCCTCGACCACCAG***AATATCCATATCCGTCTCGG	3bp del
F020	CAGTCCCTCGACCACCAGT****ATCCATATCCGTCTCGG	5bp del
F029	CAGTCCCTCGACCA** <u>(63del + 7bp ins)</u> **CTTTTC	56bp del
F035	CAGTCCCTCGACCACCAGT***TATCCATATCCGTCTCGG	3bp del
F036	CAGTCCCTCGACCACCAGTGAAT <u>GGAA</u> TATCCATATCCGTCTCGG	5bp ins
F041	CAGTCCCTCGACCACCAG****ATATCCATATCCGTCTCGG	4bp del
F043	CAGTCCCTCGACCACCA*****TATCCATATCCGTCTCGG	6bp del
F047	CAGTCCCTCGACCACCAGT* <u>AATATCCATATCCGTCTCGG</u>	1bp del
F050	CAGTCCCTCGACCACCAG**GAATATCCATATCCGTCTCGG	2bp del
F074	CAGTCCCTCGACCACCAGTGAA*ATCCATATCCGTCTCGG	1bp del
F098	CAGTCCCTCGACCACCAG****ATATCCATATCCGTCTCGG	4bp del

Table 1. Sequencing assay for ZFN-induced mutations in the FBN1-targeted region. Multiple deletions or insertions depicted using asterisks or underlines, respectively.

<i>In vitro</i> development of SCNT embryos				
SCNT embryos reconstructed	395	334		
Early cleavage-stage embryos	302	272 ^b		
Blastocyst-stage embryos on day 5	245 ^a	–		
Production of heterozygous <i>FBN1</i> mutant cloned piglets				
Recipient	#R1 ^a	#R2 ^a	#R3 ^b	#R4 ^b
Embryos transferred	103	103	136	136
Pregnancy	+	+	+	+
No. of viable cloned piglet	4	3	2	8
No. of stillborn cloned piglet	0	1	1	0

Table 2. *In vitro* development of SCNT embryos and production of heterozygous *FBN1* mutant cloned piglets. ^aThe SCNT embryos cultured for 5 to 6 days were transferred to the recipients' uteri. ^bThe SCNT embryos cultured for 1 to 2 days were transferred to the recipients' oviducts.

the elastic fibres of the aortic medial tissues of the *FBN1* mutant piglets (Fig. 3E,F) exhibited fragmented, discontinuous structures. Furthermore, there was only a sparse collagenous connective tissue layer within the elastic fibre structure (Fig. 3E,F). Immunohistochemical analyses using anti-FBN1 and anti-FBN2 antibodies revealed that the intensity of FBN1-positive microfibrils was lower in the aortic wall medial tissue of the *FBN1* mutant cloned piglets (Fig. 3G) compared with those from the WT piglets (Fig. 3C). In contrast, FBN2 was detected in the tissues of the *FBN1* mutant cloned piglets (Fig. 3H), although it was undetectable in those of the WT controls (Fig. 3D). These histological abnormalities were not detected in the distal thoracic aorta.

Dilation of the sinus of Valsalva and proximal thoracic aorta, as observed in patients with MFS, was not observed in these pigs. No individuals were found to have developed the ectopia lentis generally observed in patients with MFS. Two of the 7 live cloned offspring grew normally beyond sexual maturity.

Piglet No.	Birth weight (kg)	Postpartum survival (day)	Neonatal phenotypic abnormalities	Phenotypic features
Embryo transfer at 5 or 6 days				
#1	1.088	551 ^e	–	Quadriplegia
#2	1.051	19 ^u	+	Fragmentation of elastic fibers*, Pectus excavatum*
#3	0.550	68 ^u	–	
#4	0.536	1 ^e	+	Cleft palate, Fragmentation of elastic fibers*, Pectus excavatum*
#5	0.858	738 ^e	–	
#6	0.911	3 ^u	+	Delayed bone mineralization*
#7	0.944	0 ^s	+	Cleft palate
#8	0.811	0 ^u	–	
Embryo transfer at 1 or 2 days				
#9	1.481	90 ^e	–	Quadriplegia
#10	1.247	520 ^e	–	Pectus excavatum*, Quadriplegia
#11	0.506	0 ^s	–	
#12	0.855	4 ^u	–	
#13	0.956	76 ^e	–	Distressed breathing, Quadriplegia
#14	0.605	0 ^u	–	
#15	0.875	412 ^e	–	Scoliosis*
#16	1.210	3 ^u	–	
#17	1.158	0 ^e	–	
#18	0.781	38 ^u	–	
#19	0.849	66 ^e	–	Nystagmus, Quadriplegia

Table 3. Phenotypes of heterozygous *FBN1* mutant cloned piglets. ^eEuthanatized. ^sStillborn. ^uThe cause of death is unknown. *Marfan-like symptoms.

Phenotypes of heterozygous *FBN1* mutant cloned pigs derived from early-cleavage stage embryos. No external abnormalities were apparent in any of the 11 *FBN1* mutant neonates (including 1 still-born) obtained after transfer of the cloned embryos at the early cleavage stages (Table 3). CT analysis of 5 piglets within 4 days after birth detected no skeletal abnormalities.

Three of the cloned pigs exhibited symptoms of gait disturbance, nystagmus, distressed breathing, and quadriplegia and were therefore euthanized at ages ranging from 66 to 90 days. The cause of these abnormalities was unknown.

Two pigs grew to beyond sexual maturity. One was found to exhibit a spinal deformity (Fig. 4B) and abnormal gait at 145 days of age. This pig exhibited astasia at 399 days of age and was therefore euthanized. Scoliosis of the spine was recognized at autopsy, and a CT scan of the spinal column revealed that the normal vector of the plane formed by the superior margin and that of the plane formed by the inferior margin of the lumbar vertebra (second lumbar: L2) were offset by 6.5° (normal alignment in pigs, 1.5°) as shown in Fig. 4C,D. The other pig was euthanized at 520 days of age when it exhibited astasia. Pectus excavatum was found at autopsy, although it was not apparent at the neonatal stage.

Generation of heterozygous and homozygous *FBN1* mutant progeny. We mated heterozygous *FBN1* mutant cloned pigs (founder males) and WT females to produce male and female heterozygous *FBN1* mutant offspring in the first-generation (G1) progeny (Fig. S3). Additionally, the G2 progeny were generated by mating the G1 animals (Fig. S1D, S3, S7A). The G2 offspring comprised homozygous *FBN1* mutants, heterozygous *FBN1* mutants, and wild-type individuals, per Mendelian inheritance principles. The incidence (3 of 12, Table S1) of the heterozygous *FBN1* mutant pigs exhibiting the MFS-like symptoms in the G1 and G2 progeny was similar to that in the founder cloned pigs generated from the short-cultured SCNT embryos (2 of 11). The G2 homozygous mutant pigs showed typical symptoms of MFS, such as dilatation of the ascending aorta and rupture of the elastic lamina (Fig. S4), aortic dissection (Fig. S5), ectopia lentis (Fig. S6), and lipodystrophy (Fig. S7). Similar to the MFS mouse model^{10–12}, the homozygous mutation conferred neonatal lethality (longest survival time: 28 days). Furthermore, by examining the levels of *FBN1* mRNA expressed in fibroblasts isolated from these animals, we confirmed that the mRNA had been degraded, probably through a nonsense-mediated mRNA decay (NMD) mechanism (Fig. S8).

Discussion

There are more than 3,000 documented mutations of human *FBN1* (<http://www.umd.be/FBN1/>). Patients with MFS with a heterozygous *FBN1* mutation that generates a truncated form of *FBN1* (Arg429X, Tyr434X) exhibit typical MFS pathology of the skeleton, eyes, and blood vessels as well as symptoms of scoliosis and dilation of the arteries^{28,29}. In the present study, to develop an animal model to better understand the pathogenesis of MFS, we generated cloned pigs heterozygous for a mutant *FBN1* (Glu433AsnfsX98).

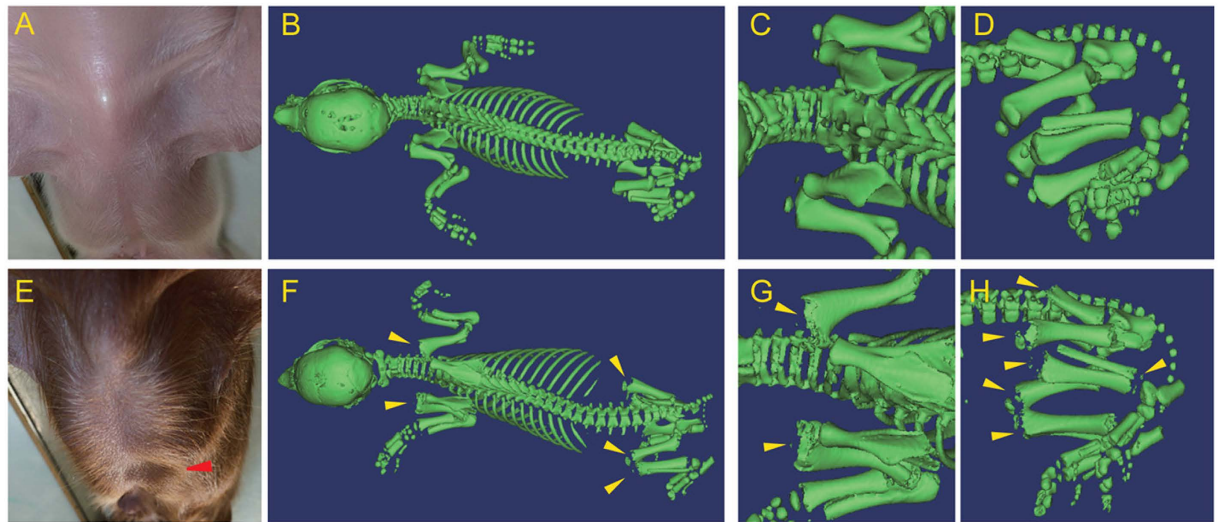


Figure 2. Skeletal abnormalities of the heterozygous *FBNI* mutant cloned pigs. (A,E) Appearance of the thorax of a WT pig (A) and an *FBNI* mutant pig with pectus excavatum (E, red arrowhead). (B–D,F–H) Multidetector CT imaging of the skeletal structures of a WT piglet (B–D) and an *FBNI* mutant piglet (#6, F–H). The WT and *FBNI* mutant piglets had a barrel-shaped (B) and a conically shaped (G) thorax, respectively. Delayed mineralization of the primary spongiosa and epiphyseal nucleus (arrowhead) was recognized in the humerus (G), the os coxa (H), the femur (H), and the fibula (H) of the *FBNI* mutant piglet.

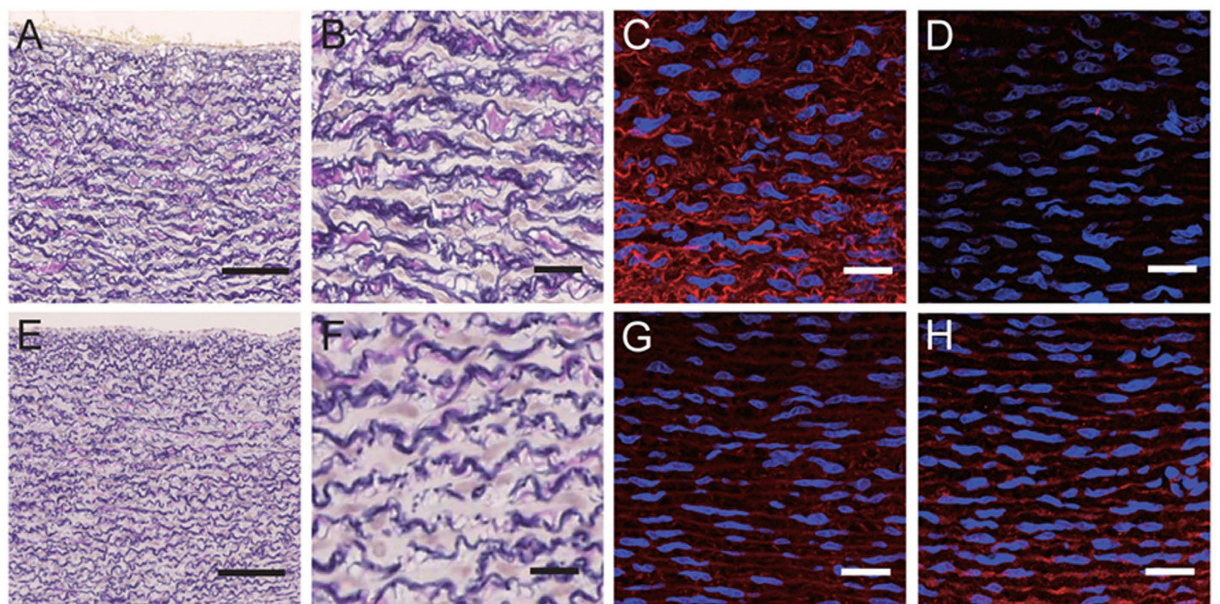


Figure 3. Histology of the proximal thoracic aortic wall of the heterozygous *FBNI* mutant cloned piglets. Proximal thoracic aortic wall of WT (A–D) and heterozygous *FBNI* mutant cloned piglets (E–H). EVG-stained sections from the *FBNI* mutant cloned piglets (E,F) show that the elastic fibres had a fractured and discontinuous structures compared with those of wild-type (WT) piglets (A,B). (C,G) The intensity of staining of FBN1-positive microfibrils was reduced in the aortic wall medial tissue of the mutant piglets (G) compared with that of WT piglets (C). (D,H) FBN2 was undetectable in the aortic wall medial tissue of the WT piglets (D), whereas it was clearly detected in the same tissue of *FBNI* mutant piglets (H). Nuclear staining (DAPI) is shown in blue (C,D,G,H). Scale bars: 100 μm (A,E) and 20 μm (B–D,F–H).

In the present study, heterozygous *FBNI* mutant cloned pigs were generated from a single line of nuclear donor cells; therefore, all cloned animals were siblings with the same genetic background and the same mutation. However, the cloned piglets did not exhibit a homogenous phenotype. The relationship between MFS genotype and the phenotype is extremely complex, and there are differences in pathology between patients of the same family lineage³⁰. Moreover, heterozygous *FBNI* knockout (KO) mice carrying the same mutation exhibit

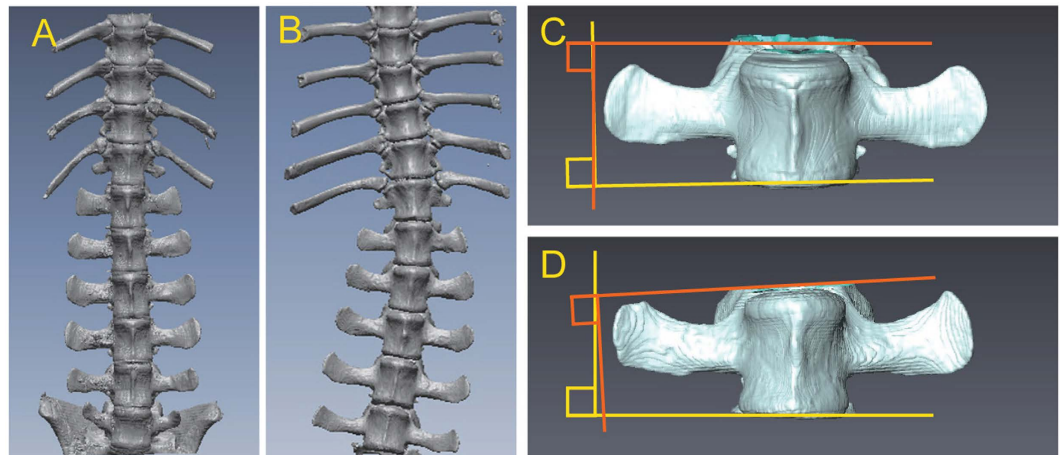


Figure 4. Scoliosis of a *FBNI* mutant cloned pig. (A,B) CT image of an *FBNI* mutant cloned pig (#15, B) showing scoliosis of the spine, compared with a WT pig (A). (C,D) CT images of the lumbar vertebrae (L2) of an *FBNI* mutant cloned pig with scoliosis (D) indicated that the normal vector of the plane formed by the superior margin of the vertebra and that of the plane formed by the inferior margin were offset by 6.5°. Normal alignment in a WT pig (C) was 1.5°.

lineage-specific phenotypic differences, and the severity of disease correlates negatively with the level of *FBNI* mRNA expression. These findings suggest the contribution of both epigenetic and genetic factors to the expression of MFS phenotypes and the severity of symptoms¹³.

Immediately following fertilization, paternal genomic DNA undergoes rapid and progressive demethylation, whereas the maternal genomic DNA undergoes gradual demethylation after postfertilization S-phases^{31,32}. Demethylation progresses until the late morula stage (day 4) followed by remethylation of genomic DNA^{31,32}. Evidence indicates that the characteristic genomic demethylation–methylation pattern that occurs during early development is affected by *in vitro* culture of embryos. For example, pig embryos cultured *in vitro* and embryos that develop *in utero* differ in their expression of 588 genes³³. In the present study, we generated cloned pigs from embryos cultured for 1–2 or 5–6 days. Cloned animals derived from the latter cultures more frequently exhibited MFS-like phenotypes. Epigenetic regulatory patterns of transcription are determined early during embryogenesis³¹. Together, these findings suggest that epigenetic factors might have influenced the phenotypes of the *FBNI* mutant cloned pigs generated here. Therefore, we suggest that these differences in phenotypes can be attributed to lower levels of *FBNI* mRNA synthesized by the single WT allele and that efficient generation of porcine models of MFS may require regulation of epigenetic modifiers in addition to mutation of the causal gene. The transcriptional activity of the WT allele in heterozygous *FBNI* mutant pigs needs to be analysed.

To correctly assess the effects of heterozygous *FBNI* mutation in pigs, founder cloned pigs were crossbred with WT pigs to obtain progeny animals, followed by analysis of the offspring's phenotypes. Because methylation of genomic DNA is normalized by sexual reproduction, this crossbreeding must have eliminated the unnatural epigenetic regulation that resulted from SCNT^{31,32}. Analysis of the progeny animals therefore enabled us to confirm the influence of the mutant gene in isolation. The heterozygous *FBNI* mutation transmitted from the founder cloned pigs to their progeny caused the similar pathological phenotypes, thereby indicating the significance of this mutation in the pig.

In contrast, dominant incidence of the abnormal phenotype in the founder cloned animals generated from the long-cultured SCNT embryos compared to the progeny animals and the clones derived from the short-cultured embryos further indicated the epigenetic influence on the outcome of the heterozygous *FBNI* mutation.

Scoliosis is a major symptom of MFS and affects more than 60% of patients, and 25–50% of these patients suffer from severe deformities that require surgery³⁴. However, the incidence of scoliosis in *FBNI* mutant pigs studied here was lower than that in patients with MFS, and the spinal deformation was less severe. For example, studies of animal models of idiopathic scoliosis indicate that the lower incidence of scoliosis in quadrupedal animals results from the different directional gravitational force on the spine³⁵ between bipedal humans and quadrupedal pigs. Therefore, this difference likely resulted in the lower incidence and reduced severity of scoliosis in the *FBNI* mutant pigs.

Delayed mineralization of the epiphysis occurred in the *FBNI* mutant pigs studied here, which is consistent with studies of mice showing that *FBNI* expression levels influence bone density. For example, bone volume is reduced in *Fbn1*^{MgR/MgR} mice, which express only 15% of the normal level of *FBNI* because of TGF- β -induced osteoclastogenesis³⁶. Furthermore, bone mineral density and volume are lower in *FBNI*-KO mice than in normal mice¹⁴, and patients with MFS display reduced mineral density of the epiphysis; however, whether or not this contributes to pathogenesis is unknown³⁷. Therefore, a detailed analysis of the bone formation abnormalities that occur in *FBNI* mutant pigs will likely help explain the symptomatology of patients with MFS.

Histopathology of the thoracic aorta is an important characteristic of MFS. For example, dilation of the aorta occurs in 78% of patients with MFS³⁸, and enlargement of the aorta and formation of aneurysms may lead to aortic

rupture. In patients with MFS with aortic aneurisms, fragmentation of the elastic fibres was evident³⁹. Here we observed fragmentation of elastic fibres in the *FBN1* mutant pigs.

Elastic fibres are composed of an elastin core surrounded by microfibrils⁴⁰. FBN2 is present near the centre of the microfibrils, surrounded by FBN1^{41,42}. Consequently, when centrally located FBN2 epitopes appear exterior to the microfibrils, reaction with anti-FBN2 antibodies is induced. We show here using immunohistochemistry that the tunica media of the thoracic aorta of heterozygous *FBN1* mutant cloned pigs expressed low levels of FBN1 but high levels of FBN2. These findings may be explained as follows: (1) the amount of FBN1 decreased because the *FBN1* mRNA had been degraded, and (2) FBN2 molecules near the central parts of the microfibrils were not covered by a sufficient amount of normal FBN1.

In the present study, we generated pigs that were heterozygous for a mutant *FBN1* and exhibited phenotypes resembling the symptoms of human MFS. Furthermore, two groups of cloned siblings with mutated *FBN1* on a syngeneic background showed striking differences in their individual phenotypes, which is consistent with the distinct phenotypes of familial cases of patients with MFS. The manner in which the expression of FBN1 from the remaining allele is regulated is likely critical for establishing the heterozygous *FBN1* mutant pig as a model for human MFS. Consequently, the heterozygous *FBN1* mutant pigs that we generated in the present study will likely prove useful for investigation of the epigenetic modifiers of MFS onset.

Material and Methods

Animal care. The Institutional Animal Care and Use Committee of Meiji University approved the animal experiments described in this study (IACUC12-0008). All animal care and experimental procedures were performed in accordance with Japan Act on Welfare and Management of Animals and regulations. Six crossbred (Large White/Landrace × Duroc) prepubertal gilts served as surrogate mothers for the embryo transfer experiments or as breeder pigs for progeny production. Three male crossbred new-born piglets were used as controls for the *FBN1* mutant cloned piglets. Pigs were housed in a temperature-controlled room, had free access to water and were provided with growth-stage appropriate commercial feed (Chubushiryō Co., Ltd. Nagoya, Japan) in accordance with the Japanese Feeding Standard for Swine (2005)⁴³. The health of all pigs was assessed at feeding (08:00 and 17:00). For autopsies, piglets were anaesthetized using intramuscular injection of ketamine (11 mg/kg, Fujita Pharmaceutical Co., Ltd., Tokyo, Japan). Anaesthesia was maintained via inhalation of isoflurane (DS Pharma animal Health Co., Ltd., Osaka, Japan), and the piglets were exsanguinated. Adult pigs were administered intramuscular injection of 1% mafoprazine mesylate (0.5 mg/kg, DS Pharma animal Health Co., Ltd.) followed by intravenous pentobarbital (Kyoritsu Seiyaku Co., Ltd., Tokyo, Japan), and anaesthesia was maintained via inhalation of isoflurane while the pigs were exsanguinated.

Chemicals. All chemicals were purchased from the Sigma-Aldrich Chemical Co. (St. Louis, MO, USA) unless otherwise indicated.

Design of ZFNs. A custom ZFN mRNA for porcine *FBN1* was obtained from Sigma-Aldrich Chemical Co. The supplier designed and validated the ZFN mRNAs. Each ZFN contained six zinc finger domains recognizing 18 bases (Fig. 1). These sequences displayed high specificity, such that if fewer than 9 of the 36 bases were mismatched, off-target sequences were not recognized. This specificity was confirmed using the porcine genome DNA database Sscrofa9 Ensembl (http://feb2012.archive.ensembl.org/Sus_scrofa/Info/Index) (Table S2).

Isolation of *FBN1* mutant cells and culture conditions. A primary culture of porcine foetal fibroblasts (male, Large White/Landrace × Duroc) was used to isolate *FBN1* mutant cells. The fibroblasts and their derivatives (mutant cells) were seeded on type I collagen-coated dishes or plates (Asahi Glass, Tokyo, Japan) and were cultured in MEM α (Life Technologies, Carlsbad, CA, USA) supplemented with 15% foetal bovine serum (FBS, Nichirei Bioscience, Tokyo, Japan) and 1 \times antibiotic-antimycotic solution (Life Technologies) in a humidified atmosphere containing 5% CO₂ at 37 °C. The foetal fibroblasts were cultured to 70–90% confluence, washed twice with D-PBS(–) (Life Technologies) and treated with 0.05% trypsin-EDTA (Life Technologies) to isolate and collect the cells. The cells (4 \times 10⁵) were then suspended in 40 μ L of R buffer (a component of the Neon Transfection System, Life Technologies), and 2 μ L of ZFN-encoding mRNA solution (400 ng/ μ L in RNase-free water) was added. The cells were electroporated as follows: pulse voltage, 1,100 V; pulse width, 30 ms; and pulse number, 1. Following electroporation, the cells were cultured at 32 °C for 3 days (transient cold shock), initially without antibiotics in the medium described above and then with antibiotics after 24 h⁴⁴. For recovery from the transient cold shock, the cells were cultured at 37 °C until they approached confluence. Five 96-well plates were used to prepare a limiting dilution of a cell suspension, and 12 days later, cells that were >50% confluent in each well were selected and subcultured.

Analysis of ZFN-induced mutations in nuclear donor cells and cloned piglets. The target region of *FBN1*-ZFNs was amplified via direct PCR from the cell clones using MightyAmp DNA polymerase (Takara Bio, Shiga, Japan) and the corresponding primers 5'-GACATAGGTGAAGACTTCGTAGG and 5'-TCACTCTCAAGACTCCAGTTTGG. Nested PCR was performed using PrimeSTAR HS DNA polymerase (Takara Bio) and the appropriate primers 5'-AACTGAGAGTGACTTCCATGGAC and 5'-GCAACCGTCAATTTCTCTATG. The nested PCR fragment from each clone was analysed using the sequencing primer 5'-TAACTTGTGCTCCAGCTCAGGTG, the BigDye Terminator Cycle Sequencing Kit and an ABI PRISM 3130xl Genetic Analyzer (Life Technologies). The nested PCR fragments that contained the mutation were subcloned into the sequencing vector pCR4Blunt-TOPO (Life Technologies).

For analysis of the mutation in each piglet, genomic DNA was extracted from tail biopsies of the piglets using a DNeasy Tissue and Blood Kit (QIAGEN, Hilden, Germany), and PCR genotyping and DNA sequencing were performed as described above.

Somatic cell nuclear transfer and embryo transfer. SCNT was performed as described previously with slight modifications²⁶. Briefly, *in vitro*-matured oocytes were enucleated via gentle aspiration of the polar body and the adjacent cytoplasm using a bevelled pipette in Tyrode lactose medium containing 10 mM HEPES and 0.3% (w/v) polyvinylpyrrolidone in the presence of 0.1 µg/mL demecolcine, 5 µg/mL cytochalasin B (CB) and 10% FBS.

Nuclear donor cells (clone F047) were used following cell-cycle synchronization induced by serum starvation for two days. A single donor cell was inserted into the perivitelline space of an enucleated oocyte. The donor cell-oocyte complexes were placed in a solution containing 280 mM mannitol (Nacalai Tesque, Kyoto, Japan), 0.15 mM MgSO₄, 0.01% (w/v) polyvinyl alcohol (PVA) and 0.5 mM HEPES (pH 7.2) and were held between two electrode needles. Membrane fusion was induced using an Electro Cell Fusion Generator (LF201; Nepa Gene, Chiba, Japan) by applying a single pulse of direct-current (DC) (267 V/mm for 20 µs) and pre- and post-pulse alternating currents of 4 V at 1 MHz for 5 s.

The reconstructed embryos were cultured in porcine zygote medium-5 (PZM-5; Research Institute for the Functional Peptides, Yamagata, Japan) supplemented with 4 mg/mL bovine serum albumin for 1 to 1.5 h, followed by electrical activation. For induction of electrical activation, the reconstructed embryos were aligned between two wire electrodes (1.0 mm apart) on a fusion chamber slide filled with the activation solution (280 mM mannitol, 0.05 mM CaCl₂, 0.1 mM MgSO₄ and 0.01% (w/v) PVA). A DC pulse of 150 V/mm was applied for 100 µs using the Electro Cell Fusion Generator. After activation, the reconstructed embryos were cultured in PZM-5 for 3 h in 5 µg/mL CB and 500 nM Scriptaid followed by culture in 500 nM Scriptaid for 12–14 h. To assess their development, the cloned embryos were next cultured in PZM-5 and divided into two groups (SCNT embryos cultured for 1–2 days or 5–6 days). Embryo culture was performed in a humidified atmosphere containing 5% CO₂, 5% O₂, and 90% N₂ at 38.5 °C. After reaching the morula stage, the embryos were cultured in PZM-5 supplemented with 10% FBS.

Crossbred prepubertal gilts weighing 100 to 105 kg were used as recipients of the SCNT embryos after synchronization of oestrus by administration of equine chorionic gonadotropin (eCG, ASKA Pharmaceutical, Tokyo, Japan) and human chorionic gonadotropin (hCG, Kyoritsu Pharmaceutical, Tokyo, Japan). The SCNT embryos at the 1- to 2-cell stage were transferred to the oviduct of the recipients after culture for 1–2 days. After culture for 5–6 days, the SCNT blastocysts were transferred to the uterine horns of the recipients. Embryos were transferred to pigs administered general anaesthesia induced using intramuscular injection of meprobazine mesylate and thiopental (10 mg/kg, DS Pharma Animal Health Co., Ltd., Osaka, Japan), and anaesthesia was maintained by administration of isoflurane gas.

CT analysis. CT analyses of the piglets were performed using a SOMATOM Sensation 16 CT scanner (Siemens AG, Munich, Germany). Piglets were subjected to CT after death. Each specimen was placed in a prone position, and noncontrast CT scans of sections 0.625-mm thick were obtained from vertical axial tomographs acquired at 0.625-mm intervals. Scan settings were 120 kVp, 400 mA, and a tube rotation time of 0.5 s. The grey-scale threshold was set to 75 to separate bone from the surrounding tissue using an adaptive threshold method. Three-dimensional (3D) models of the whole body were based on the 0.625-mm thick CT scan slices generated using Advantage Workstation 4.5 software (GE Healthcare, Waukesha, WI, USA).

Analysis of scoliosis. The spines of pigs potentially suffering from scoliosis were removed during autopsy and analysed using CT. DICOM (Digital Imaging and Communication in Medicine) data were converted to Stereolithography data using AVIZO (FEI Company, Hillsboro, OR, USA). RapidFormORX (Geomagic Inc., Morrisville, NC, USA) was used to determine the 3D coordinates of the upper and lower surfaces of each vertebral body, and these data were used to derive equations for the planes of best fit for each vertebral body. The inner product of the normal unit vectors of the upper and lower planes was calculated, the angle formed by the two planes was determined and the deformity of the lumbar vertebrae was assessed.

Histological analysis. Thoracic aortic tissues were fixed in 10%-neutral buffered formalin solution (Wako Pure Chemical Industries, Osaka, Japan), embedded in paraffin, sectioned, and treated with EVG stain using standard methods. The primary antibodies used were an anti-FBN1 polyclonal antibody (provided by Prof. Tomoyuki Nakamura, Kansai Medical University)⁴⁵ and an anti-FBN2 polyclonal antibody (provided by Dr. Lynn Sakai, Shriner Institute)⁴². The secondary antibody used was an Alexa Fluor 555-conjugated anti-rabbit IgG (Life Technologies), and the nuclei were stained with 4',6-diamidino-2-phenylindole (DAPI). Images were acquired using a confocal microscope with 488- and 543-nm filters (LSM780; Carl Zeiss MicroImaging, Jena, Germany).

References

- Sakai, L. Y., Keene, D. R. & Engvall, E. Fibrillin, a new 350-kD glycoprotein, is a component of extracellular microfibrils. *J Cell Biol* **103**, 2499–2509 (1986).
- Robinson, P. N. & Booms, P. The molecular pathogenesis of the Marfan syndrome. *Cell Mol Life Sci* **58**, 1698–1707 (2001).
- Ramirez, F. & Dietz, H. C. Fibrillin-rich microfibrils: Structural determinants of morphogenetic and homeostatic events. *J Cell Physiol* **213**, 326–330 (2007).
- Neptune, E. R. *et al.* Dysregulation of TGF-beta activation contributes to pathogenesis in Marfan syndrome. *Nat Genet* **33**, 407–411 (2003).
- Kaartinen, V. & Warburton, D. Fibrillin controls TGF-beta activation. *Nat Genet* **33**, 331–332 (2003).
- Dietz, H. C. *et al.* Marfan syndrome caused by a recurrent de novo missense mutation in the fibrillin gene. *Nature* **352**, 337–339 (1991).
- Lee, B. *et al.* Linkage of Marfan syndrome and a phenotypically related disorder to two different fibrillin genes. *Nature* **352**, 330–334 (1991).
- Dean, J. C. Marfan syndrome: clinical diagnosis and management. *Eur J Hum Genet* **15**, 724–733 (2007).
- Canadas, V., Vilacosta, I., Bruna, I. & Fuster, V. Marfan syndrome. Part 1: pathophysiology and diagnosis. *Nat Rev Cardiol* **7**, 256–265 (2010).

10. Pereira, L. *et al.* Targetting of the gene encoding fibrillin-1 recapitulates the vascular aspect of Marfan syndrome. *Nat Genet* **17**, 218–222 (1997).
11. Judge, D. P. *et al.* Evidence for a critical contribution of haploinsufficiency in the complex pathogenesis of Marfan syndrome. *J Clin Invest* **114**, 172–181 (2004).
12. Carta, L. *et al.* Fibrillins 1 and 2 perform partially overlapping functions during aortic development. *J Biol Chem* **281**, 8016–8023 (2006).
13. Lima, B. L. *et al.* A new mouse model for marfan syndrome presents phenotypic variability associated with the genetic background and overall levels of Fbn1 expression. *PLoS One* **5**, e14136 (2010).
14. Cook, J. R. *et al.* Generation of Fbn1 conditional null mice implicates the extracellular microfibrils in osteoprogenitor recruitment. *Genesis* **50**, 635–641 (2012).
15. Yang, D. *et al.* Generation of PPARgamma mono-allelic knockout pigs via zinc-finger nucleases and nuclear transfer cloning. *Cell Res* **21**, 979–982 (2011).
16. Hauschild, J. *et al.* Efficient generation of a biallelic knockout in pigs using zinc-finger nucleases. *Proc Natl Acad Sci USA* **108**, 12013–12017 (2011).
17. Lutz, A. J. *et al.* Double knockout pigs deficient in N-glycolylneuraminic acid and galactose alpha-1,3-galactose reduce the humoral barrier to xenotransplantation. *Xenotransplantation* **20**, 27–35 (2013).
18. Watanabe, M. *et al.* Generation of interleukin-2 receptor gamma gene knockout pigs from somatic cells genetically modified by zinc finger nuclease-encoding mRNA. *PLoS One* **8**, e76478 (2013).
19. Carlson, D. F. *et al.* Efficient TALEN-mediated gene knockout in livestock. *Proc Natl Acad Sci USA* **109**, 17382–17387 (2012).
20. Lee, K. *et al.* Engraftment of human iPS cells and allogeneic porcine cells into pigs with inactivated RAG2 and accompanying severe combined immunodeficiency. *Proc Natl Acad Sci USA* **111**, 7260–7265 (2014).
21. Tan, W. *et al.* Efficient nonmeiotic allele introgression in livestock using custom endonucleases. *Proc Natl Acad Sci USA* **110**, 16526–16531 (2013).
22. Whitworth, K. M. *et al.* Use of the CRISPR/Cas9 system to produce genetically engineered pigs from *in vitro*-derived oocytes and embryos. *Biol Reprod* **91**, 78 (2014).
23. Li, P. *et al.* Efficient generation of genetically distinct pigs in a single pregnancy using multiplexed single-guide RNA and carbohydrate selection. *Xenotransplantation* **22**, 20–31 (2015).
24. Zhou, X. *et al.* Generation of CRISPR/Cas9-mediated gene-targeted pigs via somatic cell nuclear transfer. *Cell Mol Life Sci* **72**, 1175–1184 (2015).
25. Kurome, M. *et al.* Production efficiency and telomere length of the cloned pigs following serial somatic cell nuclear transfer. *J Reprod Dev* **54**, 254–258 (2008).
26. Matsunari, H. *et al.* Transgenic-cloned pigs systemically expressing red fluorescent protein, Kusabira-Orange. *Cloning Stem Cells* **10**, 313–323 (2008).
27. Watanabe, M. *et al.* Production of transgenic cloned pigs expressing the far-red fluorescent protein monomeric Plum. *J Reprod Dev* **61**, 169–177 (2015).
28. Liu, W. O., Oefner, P. J., Qian, C., Odom, R. S. & Francke, U. Denaturing HPLC-identified novel FBN1 mutations, polymorphisms, and sequence variants in Marfan syndrome and related connective tissue disorders. *Genet Test* **1**, 237–242 (1997).
29. Rommel, K., Karck, M., Haverich, A., Schmidtke, J. & Arslan-Kirchner, M. Mutation screening of the fibrillin-1 (FBN1) gene in 76 unrelated patients with Marfan syndrome or Marfanoid features leads to the identification of 11 novel and three previously reported mutations. *Hum Mutat* **20**, 406–407 (2002).
30. Potter, K. J. *et al.* The c.7409G > A (p.Cys2470Tyr) Variant of FBN1: Phenotypic Variability across Three Generations. *Mol Syndromol* **4**, 125–135 (2013).
31. Yang, X. *et al.* Nuclear reprogramming of cloned embryos and its implications for therapeutic cloning. *Nat Genet* **39**, 295–302 (2007).
32. Cao, Z. *et al.* Dynamic reprogramming of 5-hydroxymethylcytosine during early porcine embryogenesis. *Theriogenology* **81**, 496–508 (2014).
33. Bauer, B. K. *et al.* Transcriptional profiling by deep sequencing identifies differences in mRNA transcript abundance in *in vivo*-derived versus *in vitro*-cultured porcine blastocyst stage embryos. *Biol Reprod* **83**, 791–798 (2010).
34. Gjolaj, J. P. *et al.* Spinal deformity correction in Marfan syndrome versus adolescent idiopathic scoliosis: learning from the differences. *Spine (Phila Pa 1976)* **37**, 1558–1565 (2012).
35. Janssen, M. M., de Wilde, R. F., Kouwenhoven, J. W. & Castelein, R. M. Experimental animal models in scoliosis research: a review of the literature. *Spine J* **11**, 347–358 (2011).
36. Nistala, H. *et al.* Differential effects of alendronate and losartan therapy on osteopenia and aortic aneurysm in mice with severe Marfan syndrome. *Hum Mol Genet* **19**, 4790–4798 (2010).
37. Haine, E. *et al.* Muscle and bone impairment in children with Marfan syndrome: correlation with age and FBN1 genotype. *J Bone Miner Res* **30**, 1369–1376 (2015).
38. Hwa, J. *et al.* The natural history of aortic dilatation in Marfan syndrome. *Med J Aust* **158**, 558–562 (1993).
39. Bunton, T. E. *et al.* Phenotypic alteration of vascular smooth muscle cells precedes elastolysis in a mouse model of Marfan syndrome. *Circ Res* **88**, 37–43 (2001).
40. Wu, D., Shen, Y. H., Russell, L., Coselli, J. S. & LeMaire, S. A. Molecular mechanisms of thoracic aortic dissection. *J Surg Res* **184**, 907–924 (2013).
41. Charbonneau, N. L. *et al.* *In vivo* studies of mutant fibrillin-1 microfibrils. *J Biol Chem* **285**, 24943–24955 (2010).
42. Charbonneau, N. L. *et al.* Microfibril structure masks fibrillin-2 in postnatal tissues. *J Biol Chem* **285**, 20242–20251 (2010).
43. National Agriculture and Bio-oriented Research Organization. *Japanese Feeding Standard for Swine*. (Japan Livestock Industry Association, Tokyo) (2005).
44. Doyon, Y. *et al.* Transient cold shock enhances zinc-finger nuclease-mediated gene disruption. *Nat Methods* **7**, 459–460 (2010).
45. Inoue, T. *et al.* Latent TGF-beta binding protein-2 is essential for the development of ciliary zonule microfibrils. *Hum Mol Genet* **23**, 5672–5682 (2014).

Acknowledgements

We thank Prof. Tomoyuki Nakamura and Dr. Lynn Sakai for providing the anti-fibrillin-1 and anti-fibrillin-2 polyclonal antibodies, respectively; Prof. Eiji Kobayashi, Dr. Takumi Teratani, Dr. Jiro Masubuchi and Prof. Eiji Sugimoto of Jichi Medical University for performing CT; and Dr. Yoshikazu Arai and Dr. Jun Ohgane of Meiji University for performing real-time PCR. Financial support for this study was provided by a Scientific Research Grant (A) (#15H02480 to H.N.) and (B) (#24390357 to M.M.) from the Ministry of Education, Culture, Sports, Science and Technology-Japan; by the Keio Gijyuku Academic Development Funds (to M.M.) and by the Meiji University International Institute for Bio-Resource Research (to H.N.).

Author Contributions

K.U. performed molecular and animal experiments, data acquisition, and analysis and wrote the manuscript. K.W., K.H. and M.K. contributed to data acquisition, data analysis, and interpretation in the orthopaedic research. M.W. established *FBN1* mutant cells lines. K.N. and H.M. generated cloned pigs. T.K. and M.S. contributed to data acquisition and interpretation in the histological analysis. M.N. wrote and revised manuscript. Y.A., O.S. and H.S. contributed to discussion. K.K. conceived the study and contributed to discussion. H.N. conceived and designed the study, contributed to generation of cloned pigs, and edited the manuscript. M.M. conceived and designed the study and contributed to interpretation in the orthopaedic research. All authors approved the final manuscript.

Additional Information

Supplementary information accompanies this paper at <http://www.nature.com/srep>

Competing financial interests: There is potential competing financial interest. H.S. received research grants from Daiichi Sankyo Inc. and Eisai Co. Ltd. These grants did not alter the authors' adherence to all the journal's policies on sharing data and materials.

How to cite this article: Umeyama, K. *et al.* Generation of heterozygous fibrillin-1 mutant cloned pigs from genome-edited foetal fibroblasts. *Sci. Rep.* **6**, 24413; doi: 10.1038/srep24413 (2016).



This work is licensed under a Creative Commons Attribution 4.0 International License. The images or other third party material in this article are included in the article's Creative Commons license, unless indicated otherwise in the credit line; if the material is not included under the Creative Commons license, users will need to obtain permission from the license holder to reproduce the material. To view a copy of this license, visit <http://creativecommons.org/licenses/by/4.0/>